Qin *et al. Journal of Nanobiotechnology* (2024) 22:622
https://doi.org/10.1186/s12951-024-02918-2

Journal of Nanobiotechnology

RESEARCH Open Access

Histidine phosphatase-ferroptosis crosstalk modulation for efficient hepatocellular carcinoma treatment

Yang Qin[1†], Xiaoli Ling[1†], Yunxian Li[1], Jieqiong Wang[1], Jiaqi Wang[1], Zhuoyi Rong[1], Yao Cheng[1], Zhenghao Tao[1], Haitao Zhang[1*], Hua Wei[1*] and Cui-Yun Yu[1,2*]

Abstract

Altering the mechanisms of tumor cell death and overcoming the limitations of traditional chemotherapy is pivotal to contemporary tumor treatment. Inducing ferroptosis, while circumventing safety concerns associated with ferrous vectors, through nonferrous ferroptosis is a promising but underexplored frontier in cancer therapy. Histidine phosphatase (LHPP) has emerged as a novel therapeutic target in treating hepatocellular carcinoma (HCC), but the precise mechanism of LHPP against HCC remains unclear. Herein, we explore the effects of upregulating LHPP expression on ferroptosis and tumor immunogenicity induction by simply delivering a miRNA-363-5p inhibitor (miR-363-5pi) via a previously optimized gemcitabine-oleic acid (GOA) prodrug. Efficient miRNA encapsulation was achieved through hydrogen bonding at an optimized GOA/miRNA molar feed ratio of 250:1, affording spherical nanoparticles with a uniform hydrodynamic size of 147.1 nm and a negative potential of -21.5 mV. The mechanism of this LHPP-ferroptosis crosstalk is disclosed to be an inhibited phosphorylation of the PI3K/Akt pathway, leading to a remarkable tumor inhibition rate of 88.2% in nude mice bearing Bel-7402 tumor xenografts via a combination of LHPP-triggered nonferrous ferroptosis and GOA-induced chemotherapy. The biocompatibility of GOA/miR-363-5pi is strongly supported by their non-hematologic toxicity and insignificant organ damage. In addition, the tumor immunogenic activation potential of GOA/miR-363-5pi was finally explored. Overall, this study is the first work that elucidates the precise mechanism of LHPP for treating HCC via ferroptosis induction and achieves the transformation of chemotherapy and gene therapy into ferroptosis activation with tumor cell immunogenicity, which lays a new therapeutic foundation for the clinical treatment of HCC.

†Yang Qin and Xiaoli Ling contributed equally to this work.

*Correspondence:
Haitao Zhang
zhanghaitao@usc.edu.cn
Hua Wei
weih@usc.edu.cn
Cui-Yun Yu
yucuiyunusc@hotmail.com

Full list of author information is available at the end of the article

Graphical Abstract

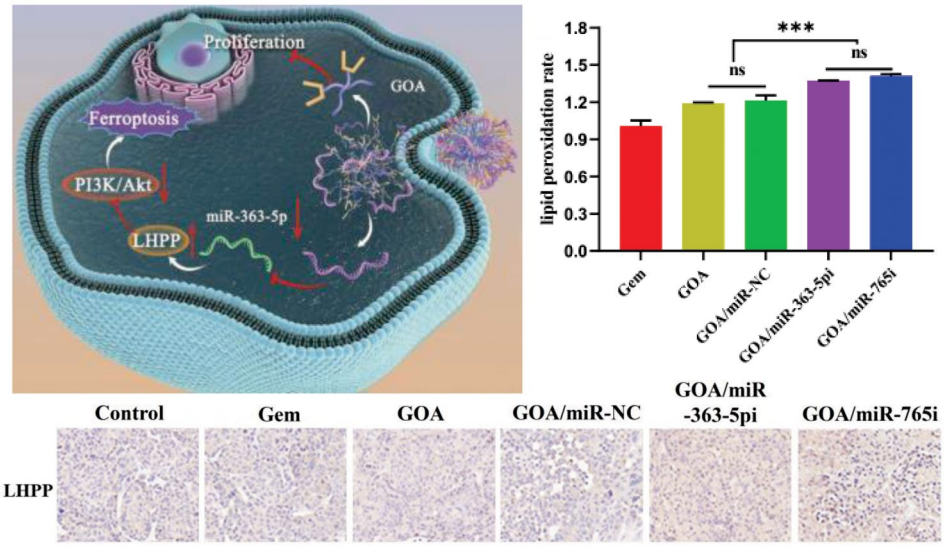

Keywords Ferroptosis, LHPP, Gemcitabine prodrug, miRNA inhibitor

Introduction

Hepatocellular carcinoma (HCC), a severe global cause of mortality [1–3], has been conventionally treated with surgery, chemotherapy, and radiotherapy [4]. However, the therapeutic efficiency of these traditional therapies remains unsatisfactory in clinics due to the inherent limitations, including high recurrence rates and serious side effects [5]. In our pursuit of optimal hepatocellular carcinoma (HCC) treatment strategies, we have achieved HCC inhibition by delivering miR-122, orchestrating a combined approach involving chemotherapy and gene therapy as recorded in [6]. Despite this, we acknowledge that the therapeutic impact remains confined. Thus, there's an impelling demand for a change of traditional cancer-fighting techniques—shifting towards innovative methods that may alter the cell death modalities or activate the immunogenicity of tumor cells.

A recently developed promising approach is shifting the cell death mode from apoptosis to ferroptosis, which is a novel form of programmed cell death induced by ferrous-dependent accumulation of lipid peroxides in cells [7–9]. As of now, most nanomedicines designed for ferroptosis have utilized ferrous nanocarriers, which elevate the concentration of intracellular Fe ions, triggering ferroptosis in cancer cells. However, they also cause toxic side effects on normal cells and organs, including chronic and acute damage [10–12]. Consequently, the use of nonferrous ferroptosis is thus an improved approach for safety considerations but remains rarely explored.

Histidine phosphatase (LHPP), a protein that removes histidine-linked phosphate groups from the proteins in healthy organ tissues, was reported to be a suppressor of HCC in 2018 [13]. Hindupur's research reveals that LHPP is predominantly localized within healthy tissues, being nearly undetectable in tumor tissues. Consequently, the deficiency of LHPP is associated with heightened tumorigenesis, whereas an enhanced expression profile of LHPP can effectively suppress the proliferation of cancer cells and safeguard liver functionality [14]. However, the specific mechanism via which LHPP affects tumors has not been fully understood, with the only disclosed fact that this action mechanism is accompanied by inactivation of the PI3K/Akt pathway [15]. Interestingly, the low PI3K/Akt pathway activity has been reported to be related to lipid peroxide accumulation in breast cancer, which serves as one of the hallmark events of ferroptosis [16]. Inspired by this promising result, it is reasonable to postulate that an upregulated LHPP expression level has the potential to induce nonferrous ferroptosis for HCC treatment.

MicroRNA (miR) has been widely used in anticancer gene therapy due to the apparent multi-target regulatory advantages [17]. Notably, the down-regulation of LHPP by miR-363-5p or miR-765 has been observed to accelerate the progression of HCC [18], indicating their potential as targets for LHPP regulation. However, miRNA is a negatively charged hydrophilic molecule that is difficult to pass through the tumor cell membranes [19]. Together with the susceptibility to degradation by nucleases with short half-lives and off-target properties, these defects of miRNAs limit their clinical applications in cancer therapy [20, 21]. Various approaches have been developed to

overcome these inherent limitations for efficient intracellular miRNA delivery. Typical examples include Kim's folic acid conjugated mixed nanoparticles for doxorubicin/miR-100c co-delivery [22] and Yu's galactosylated-chitosan-5-fluorouracil prodrug for efficient 5-FU/microRNA-122 co-delivery with enhanced chemotherapeutic sensitivity for HCC [23].

Herein, to overcome the limitations typically encountered in traditional chemotherapy gene combination therapy, a previously developed gemcitabine-oleic acid prodrug (GOA) [6] was used to deliver a miR-363-5p inhibitor (miR-363-5pi) for efficient HCC therapy via upregulated LHPP expression-activated ferroptosis. A miR-765 inhibitor (miR-765i) was used as a parallel control group. GOA and miR inhibitors formed a non-cationic nanocomplex (GOA/miR) via hydrogen bonding and hydrophobic interactions (Scheme 1). Comprehensive in vitro and in vivo evaluations were performed to demonstrate the effectiveness of both nanocomplexes in mediating ferroptosis for HCC treatment with the disclosure of the underlying mechanism.

Results and discussion

Synthesis of GOA

GOA materials were synthesized according to the previously reported methods (Fig. S1) [6] and were characterized by ^{1}H NMR spectroscopy. The successful synthesis of the intermediates was evidenced by the changes in the chemical shift (δ) values of characteristic protons in the ^{1}H NMR spectra (Fig. S2). Specifically, the chemical shift values of the methylene groups change from 2 H (CH_2OH) at δ=3.72 to 2 H (-COO-CH_2) at δ=4.36 and 3.99, respectively, due to the conversion of the neighboring groups to an ester bond, supporting the successful occurrence of an esterification reaction. Meanwhile, the appearance of the characteristic peaks assigned to oleic acid proves the successful coupling of gemcitabine and oleic acid for GOA production via an esterification condensation. Furthermore, the successful preparation of GOA is further supported by mass spectrometry, which reveals a molecular ion peak of 528 (M+H) (Fig. S3), consistent with the theoretically calculated relative molecular mass of GOA.

Preparation and characterization of GOA/miR nanocomplex

GOA/miR-NC nanocomplexes were initially prepared via a previously reported sequential denaturation annealing and nanoprecipitation method [6]. Because the hydrogen bonding interactions between GOA and miR increase with the temperature elevation, GOA/miR-NC was prepared by a programmable annealing procedure at a fixed temperature of 37℃. A molar concentration ratio of GOA to miR-NC at 250:1 or higher values led to full inhibition of miR-NC immigration in a gel retardation assay (Fig. 1A Fig. S4) due to the formation of a stabilized GOA/miR-NC nanocomplex. Note that this ratio is much greater than the previously reported stabilized ratio of 120:1 for GOA/miR-NC [6] likely due to the different base sequences of used miRNA, implying the possibility

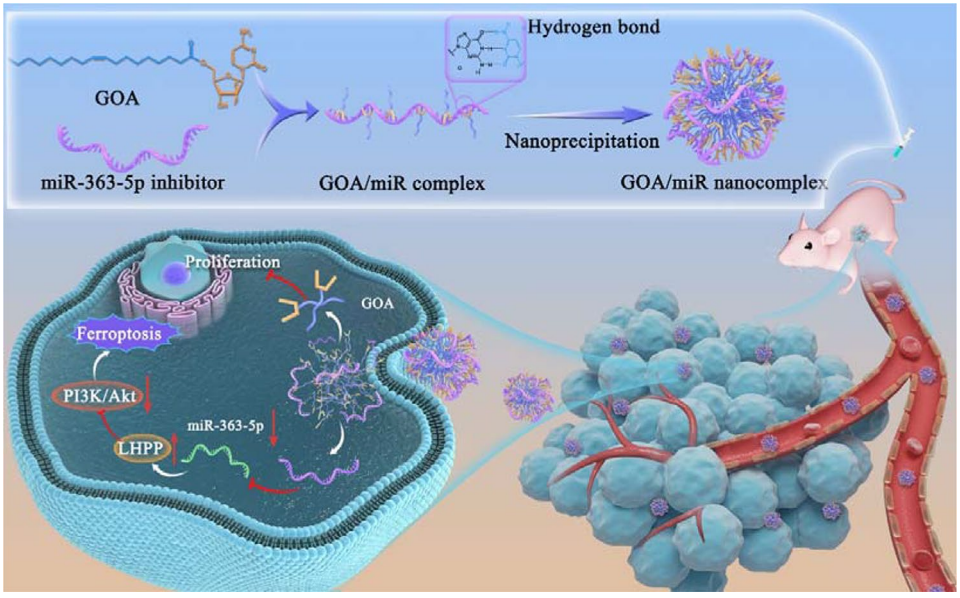

Scheme 1 Schematic illustration of the preparation and antitumor mechanism of GOA/miR nanocomplex. Preparation of GOA/miR-363-5pi nanocomplex through hydrogen bonding and hydrophobic forces. Following intravenous administration, GOA/miR-363-5pi nanocomplex selectively accumulates in murine HCC tissues and inhibits the expression of miR-363-5p, leading to an upregulation of LHPP expression, which subsequently induces ferroptosis by inactivating the PI3K/Akt pathway

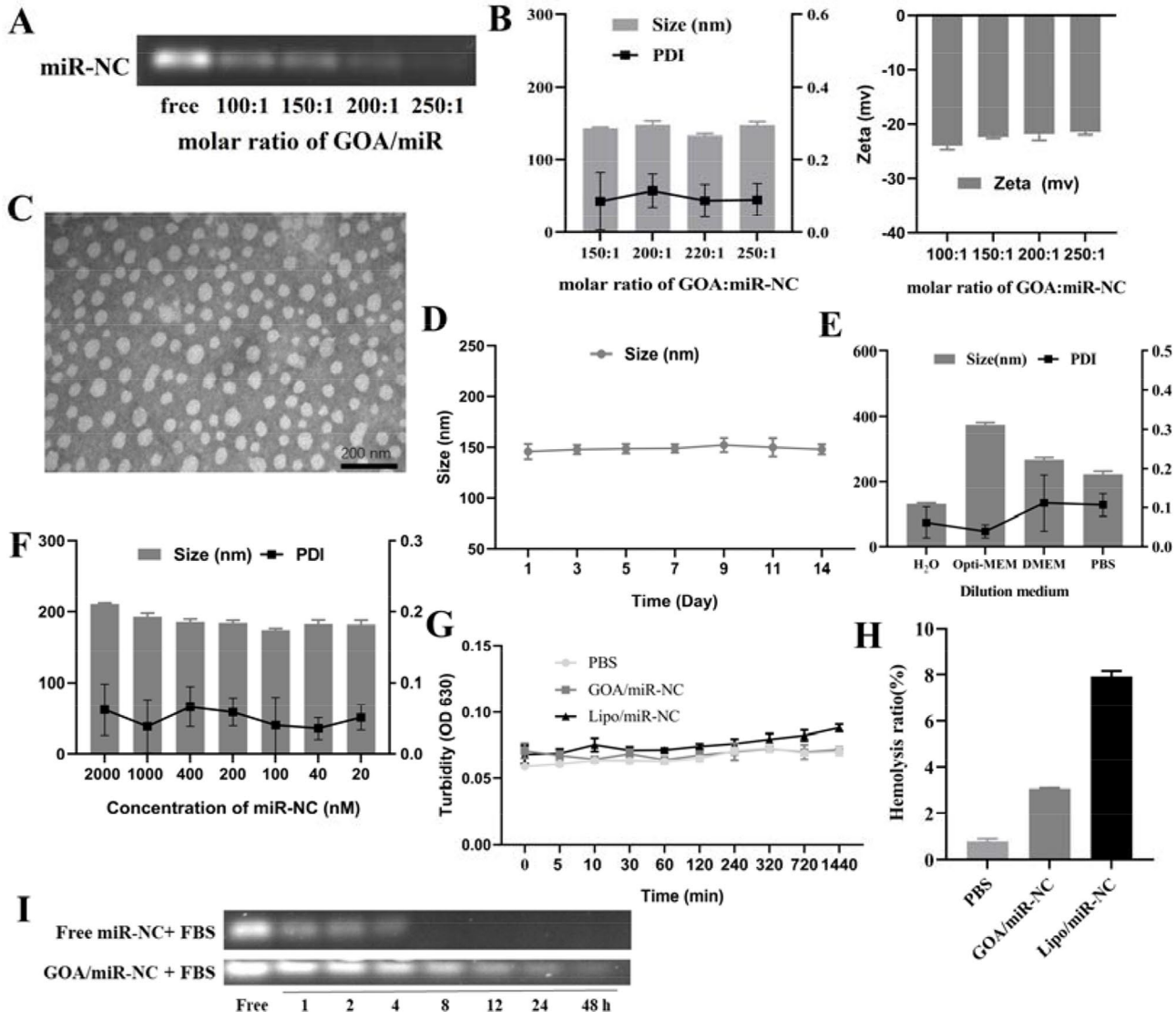

Fig. 1 Preparation and characterization of GOA/miR nanocomplex. (**A**) Gel electrophoresis bands and (**B**) particle size of GOA/miR-NC nanocomplex at different molar ratios. (**C**) Representative TEM images of GOA/miR-NC nanocomplex. Scale bars: 200 nm. (**D**) The storage stability of GOA/miR-NC nanocomplex at room temperature for 14 days. (**E**) The particle size and PDI of GOA/miR-NC nanocomplex in different media. (**F**) Dilution stability of GOA/miR-NC nanocomplex in PBS. (**G**) Protective effects of GOA/miR-NC nanocomplex on preventing aggregation induced by serum proteins. (**H**) Hemolytic effects of GOA/miR-NC nanocomplex. (**I**) Protection of miR-NC from FBS by GOA/miR nanocomplex. Data represent mean ± s.d. ($n = 3$)

of modulating the supramolecular interactions between GOA and miR-NC via varying the sequence and structure of miR-NC. Although efficient miRNA condensation was observed at a molar ratio of 250:1, a molar ratio was further optimized to afford a stabilized nanocomplex with a mean diameter smaller than 200 nm suitable for an enhanced permeation and retention (EPR) effect-mediated passive targeting to HCC. The mean diameter of all prepared GOA/miR-NC nanocomplex was determined by dynamic light scattering (DLS), which showed an average size of approximately 147.1 nm at a molar ratio of 250:1 (Fig. 1B). TEM visualization demonstrates a spherical shape with an average size of approximately 150 nm for GOA/miR-NC nanocomplex (Fig. 1C).

The colloidal stability, including storage stability, dilution, and media stability of GOA/miR-NC nanocomplex prepared at a molar ratio of 250:1 was evaluated to assess the preliminary potential as a non-cationic and non-ferrous miRNA delivery nanoplatform. Insignificant changes were observed in the particle sizes of the GOA/miR-NC nanocomplex in an aqueous phase over 14 days, indicating excellent storage stability of the GOA/miR-NC nanocomplex (Fig. 1D). The size of the nanocomplex remained unaltered at 200 nm after even a 100-fold

dilution, suggesting a favorable dilution stability that is highly desirable for intravenous administration (Fig. 1E). The salt and serum stability properties of this formulation are evidenced by the almost constant sizes at ~150 nm in water and at ~200 nm in a PBS solution irrespective of further addition of any different media, including water, PBS, Opti-MEM, and DMEM (Fig. 1F).

Next, the blood compatibility of the GOA/miR-NC nanocomplex was evaluated, which revealed insignificant OD value changes in fetal bovine serum (FBS) within 5 days (Fig. 1G) without any occurrence of red blood cell hemolysis (Fig. 1H) for the GOA/miR-NC nanocomplex. More importantly, the luminescent bands corresponding to the GOA/miR-NC nanocomplex remained detectable on the gel even after 24 h of incubation with FBS (Fig. 1I) and was further supported in the nuclease enzyme protect test (Fig. S5). The results strongly support the enhanced colloidal stability of GOA/miR nanocomplex against miRNA degradation over a relatively extended duration, which guarantees the transfection of GOA/miR nanocomplex to cancer cells in a serum-containing medium.

Preparation and characterization of GOA/miR-363-5pi nanocomplex and GOA/miR-765i nanocomplex

The preparation of GOA/miR-363-5pi and GOA/miR-765i nanocomplexes was identical to the aforementioned protocols leading to the GOA/miR-NC nanocomplex. Similarly, the formation of stabilized GOA/miR-363-5pi and GOA/miR-765i nanocomplexes for complete miR encapsulation occurred at a molar ratio of 250:1 and higher ratios (Fig. 2A and B). The optimized GOA/miR-363-5pi and GOA/miR-765i nanocomplexes show mean particle sizes of approximately 200 nm (Fig. 2C) and negative surface charges of about −20 mv (Fig. 2D). The DLS data of three prepared nanocomplexes at a molar ratio of 250:1 was summarized in Table 1, which were further

Table 1 The DLS results of the optimized three nanocomplexes. Data represent mean. ($n = 3$)

Nanocomplex	Size (nm)	PDI	Zeta (mv)
GOA/miR-NC	147.1	0.085	-21.5
GOA/miR-765i	207.6	0.112	-25.4
GOA/miR-363-5pi	208.4	0.079	-28.5

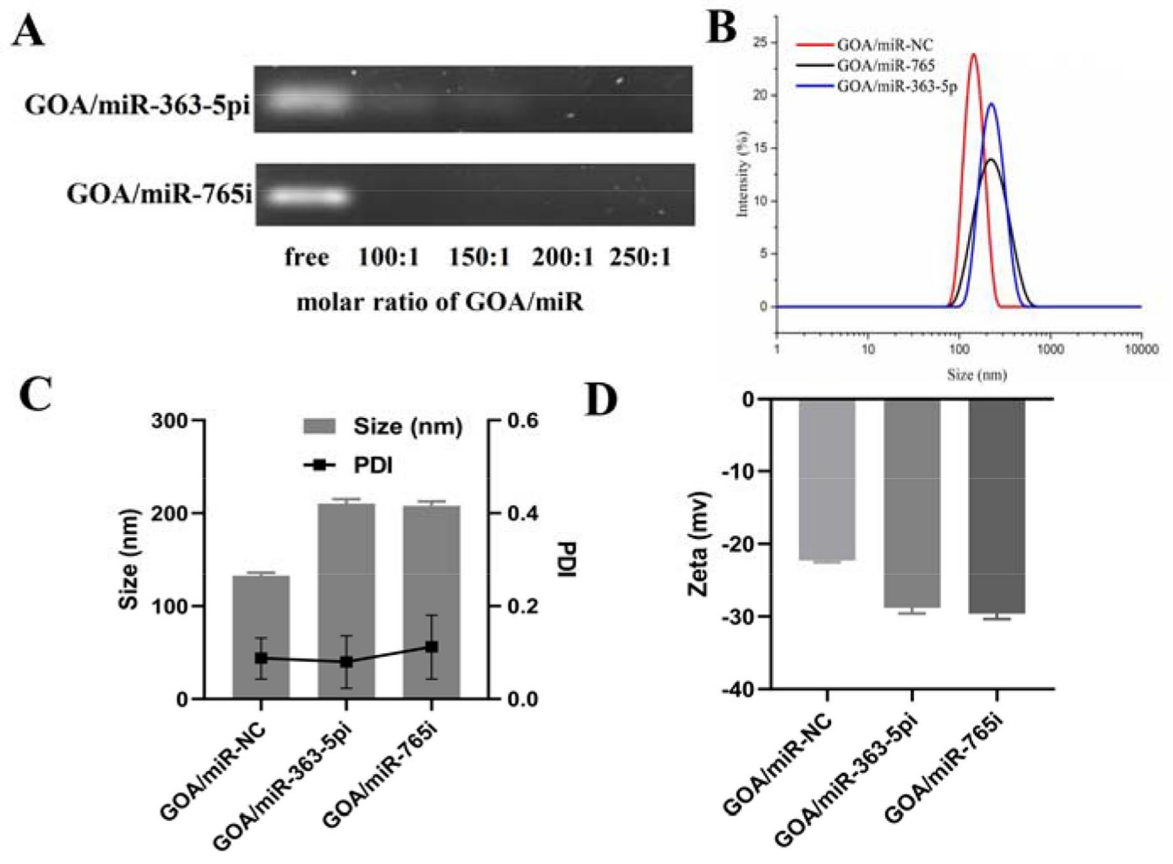

Fig. 2 Preparation and characterization of GOA/miR-363-5pi and GOA/miR-765i nanocomplex. (**A**) The gel electrophoresis bands of GOA/miR-363-5pi and GOA/miR-765i nanocomplex at various molar ratios. (**B**) The size of the GOA/miR-NC, GOA/miR-363-5pi and GOA/miR-765i nanocomplex. (**C**) The particle size and (**D**) surface potential of GOA/miR-NC, GOA/miR-363-5pi and GOA/miR-765i nanocomplex

used for subsequent in vitro and in vivo evaluations. The successful assembly of nanocomplexes with apparent negative surface charges confirms substantial miRNA encapsulation via hydrogen bonding rather than electrostatic interactions.

Cellular uptake of GOA/miR nanocomplex

Efficient cellular internalization is a prerequisite for successful miRNA delivery for specific gene silences. The cellular uptake of GOA/miR nanocomplexes was thus evaluated via flow cytometry and fluorescence microscopy. After treatment with GOA/miR nanocomplexes for 8 h, the mean fluorescence intensity in Bel-7402 cells was 1.2 and 3.4 -fold higher than those in HepG2 and SMCC-7721 cells, respectively (Fig. 3A), therefore Bel-7402 cell line was chosen as the typical HCC cell model for subsequent experiments (Fig. 3B). Note that GOA/FAM-miR-NC nanocomplexes show quite different uptake behaviors in three different HCC cell lines likely due to the inherent properties of different HCC cell lines [24–27]. Typically, the compromised cellular uptake efficiency of GOA/FAM-miR-NC

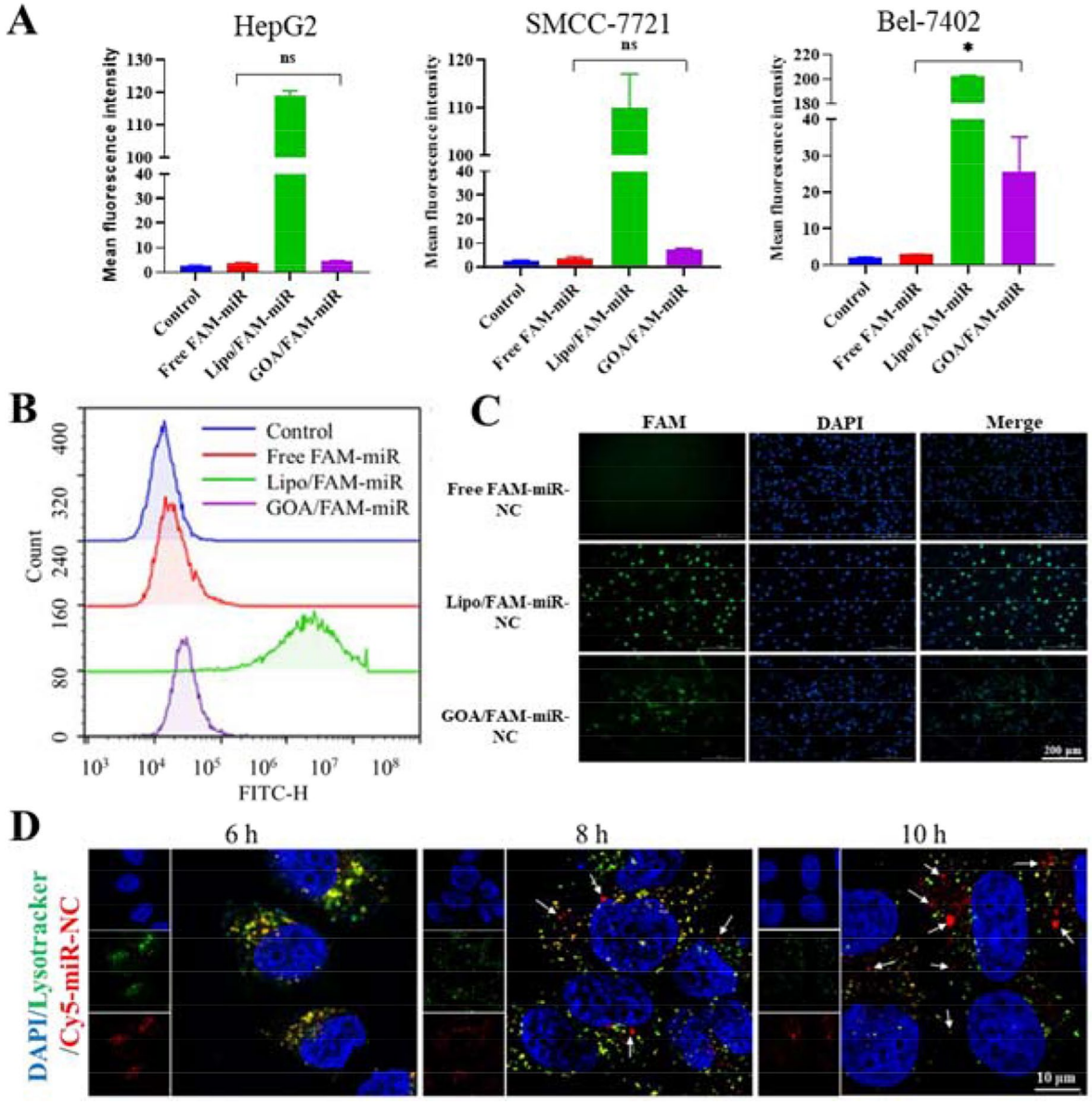

Fig. 3 Cellular uptake of GOA/miR nanocomplex. (**A**) Flow cytometry quantification of GOA/FAM-miR uptake after 8 h by three HCC cell lines, including HepG2, SMCC-721, and Bel-7402 cells. Data represent mean ± s.d. ($n = 3$). *$p < 0.05$, ns: not significant. (**B**) The representative images of flow cytometry for GOA/FAM-miR in Bel-7402 cells. (**C**) Fluorescence microscopy images of Bel-7402 cells incubated with free FAM-miR-NC, Lipo/FAM-miR-NC, and GOA/FAM-miR-NC for 8 h. miRNA concentration: 100 nM. (**D**) Confocal imaging of co-localization (yellow) of GOA/miR nanocomplex (Cy5-miR-NC, red) with lysosomes (stained with Lyso-Tracker Green, green) in Bel-7402 cells. DAPI (blue) was used for staining the nucleus. Scale bars, 10 μm

nanocomplexes in SMMC7721 and HepG2 cell lines indicates the slower uptake rates in these two cell lines compared to that in Bel-7402 cells.

Next, the endocytosis of GOA/miR nanocomplexes in Bel-7402 cells was directly visualized using fluorescence microscopy. The green fluorescence intensity of FAM in the GOA/FAM-miR group was significantly greater than that observed in the control group, indicating effective miR transportation into the cells (Fig. 3C).

The lysosomal escape ability of GOA/miR nanocomplex was further investigated. Most of the green fluorescence (lysosome stained with Lyso-Tracker Green) and red fluorescence (nanocomplexes labelled with Cy5) co-localized at 6 h, indicating that the nanocomplexes undergo an intracellular lysosome pathway after endocytosis. The red fluorescence of GOA/Cy5-miR nanocomplexes observed in the cytoplasm increased significantly after 8 h and 10 h of incubation, suggesting that the time-dependent lysosomal escape of GOA/miR nanocomplex occurs mainly after 8 h (Fig. 3D). Taken together, the GOA/miR nanocomplex is an efficient miRNA delivery vector for the Bel-7402 cell line-based HCC model.

In vitro antitumor effects

To investigate the synergistic antitumor effects of GOA/miR nanocomplex on Bel-7402 cells at different incubation periods, the inhibitory effects of GOA/miR-363-5pi nanocomplex and GOA/miR-765i nanocomplex were evaluated by MTT assays. In contrast to the insignificant inhibitory effect of free miRNA inhibitor on the growth of tumor cells, the positive Lipo group did exhibit time-dependent cytotoxicity due to the successful delivery of miR-363-5pi and miR-765i. More importantly, the nano-formulations incorporating GOA micelle components demonstrated substantial cell inhibition at 24, 48, and 72 h of incubation compared to free gemcitabine, indicating enhanced antitumor effects of gemcitabine facilitated by the delivery systems ($p<0.001$, Fig. 4A). Significantly reduced cell viabilities were recorded in the GOA/miR-363-5pi (20.3%) and GOA/miR-765i nanocomplexes (15.5%), much lower than those of GOA micelles (34.3%) and the GOA/miR-NC nanocomplex (34.3%) after an identical incubation period of 48 h ($p<0.01$). The decreased values of cell viability became even greater at a prolonged incubation duration of 72 h ($p<0.001$), strongly supporting that miR-363-5pi and miR-765i contribute to the enhanced inhibitory effect of the nanocomplexes.

To provide additional evidence on the anti-tumor properties of the nanocomplexes, an EdU incorporation assay was performed on Bel-7402 cells over 48 h. The group treated with GOA/miR-363-5pi or GOA/miR-765i nanocomplexes exhibited a significantly reduced green fluorescence intensity of EdU compared to those of the other groups (Fig. 4B), indicating a noteworthy inhibition of HCC cell proliferation induced by the GOA/miR-363-5pi

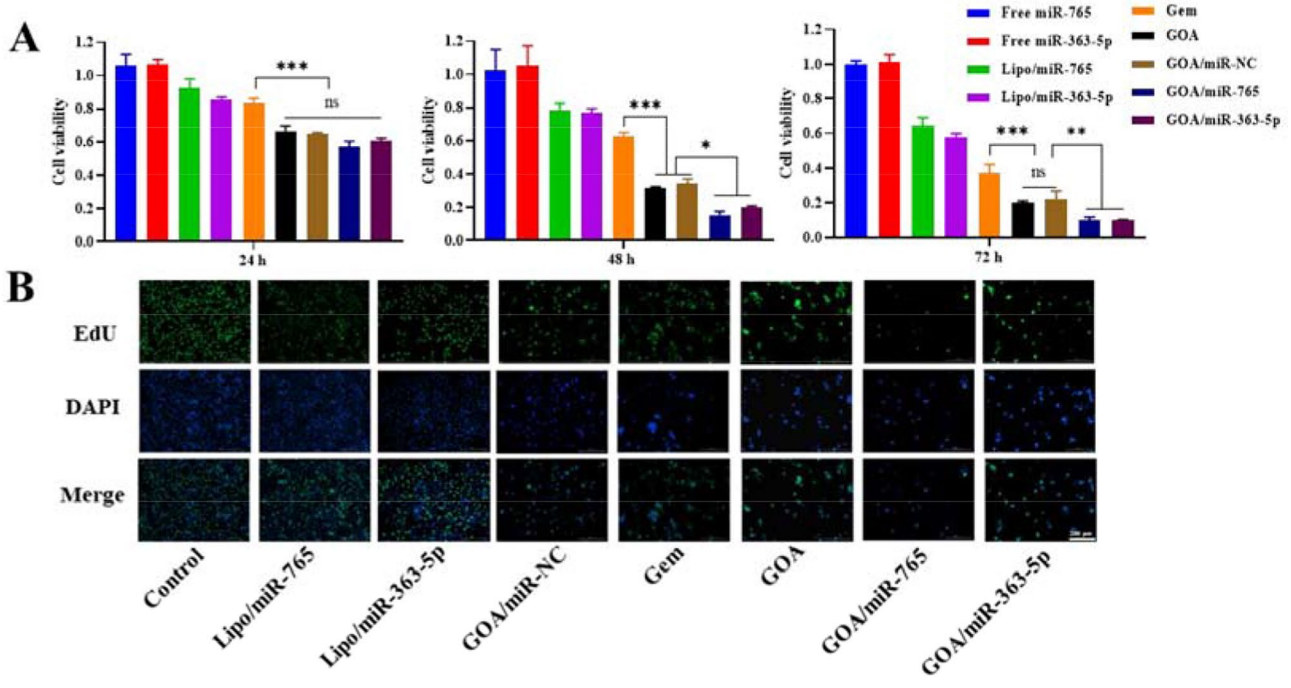

Fig. 4 In vitro antitumor effects of GOA/miR-363-5pi and GOA/miR-765i nanocomplex. (**A**) Cell viability of Bel-7402 cells incubated with different formulations after 24 h, 48 h, and 72 h. Data represent mean ± s.d. ($n=3$). *$p<0.05$, **$p<0.01$, ***$p<0.001$, ns: not significant. (**B**) Representative EdU fluorescent images on Bel-7402 cells after treatment with different formulations. Scale bar, 50 μm

or GOA/miR-765i nanocomplexes. Interestingly, the transfection of miR-363-5pi and miR-765i showed similar cell antiproliferation rates in both the MTT assay and the EdU experiment regardless of using Lipo or GOA, which suggests an equal antitumor effect by these two miRNAs.

In vitro antitumor mechanism

To verify the scientific hypothesis that GOA/miR nanocomplex induces ferroptosis by upregulating LHPP and subsequently downregulating the PI3K signaling pathway, western blotting experiments were used to investigate the alterations in proteins associated with LHPP and the PI3K pathway in tumor cells. Compared to those of the normal liver cell line L02, the decreased expression of LHPP was observed in three HCC cell lines, including HepG2, SMCC-7721, and Bel-7402 cells (Fig. 5B), which emphasizes the critical role of miRNA delivery in HCC therapy. Following 48 h of treatment with GOA/miR-363-5pi or GOA/miR-765i nanocomplexes, LHPP protein expression in Bel-7402 cells became higher than those of the other groups (Fig. 5C), suggesting the successful transfection of miR-363-5pi or miR-765i for LHPP overexpression. Interestingly, the GOA/miR-765i nanocomplex demonstrated an LHPP protein expression level similar to that of the GOA/miR-363-5pi nanocomplex. Again, the results imply similar ferroptosis effects of the two miRNAs.

LHPP can dephosphorylate the Histidine and appears to be a potential regulator of the PI3K/Akt pathway as a histidine phosphatase [15]. To elucidate the role of LHPP in the PI3K/AKT pathway, we evaluated the expression of key proteins in this pathway modulation and the respective phosphorylation levels. In comparison to those of the control groups, the protein levels involved in the PI3K/AKT pathway remained unaltered following treatment with free gemcitabine, GOA, and GOA/miR-NC, which suggests that neither gemcitabine nor GOA could make any alterations to the PI3K/AKT pathway (Fig. 5D). However, compared with those of the control group, significantly decreased levels of p-PI3K and p-Akt were observed upon transfection with GOA/miR-363-5pi or GOA/miR-765i nanocomplexes, while the PI3K or Akt levels remained consistent with values similar to that of the positive control Lipo/miR group. The deactivation of the phosphorylated PI3K/Akt pathway could be likely attributed to the successful delivery of miR-363-5pi or miR-765i for elevated LHPP expression.

Subsequently, we evaluated whether the inactivation of the PI3K/Akt pathway could trigger ferroptosis in HCC. Glutathione peroxidase4 (GPX4) expression and lipid peroxide levels were employed as typical markers to confirm ferroptosis occurrence. GPX4, with the ability to scavenge membrane lipid hydrogen peroxide products, has been identified as the central regulator of ferroptosis [28]. In comparison to the control group, lipo-mediated miR transfection significantly downregulated GPX4 protein expression, whereas Gem, GOA micelles, and GOA/miR-NC nanocomplex showed indiscernible effects on GPX4 expression, suggesting miR could downregulate the GPX4 expression regardless of gemcitabine participation (Fig. 5E). Furthermore, the gray value intensities of the GPX4 bands in the GOA/miR-363-5pi and GOA/miR-765i nanocomplex groups were lower than those of the GOA micelles and GOA/miR-NC nanocomplex groups, indicating successful miR delivery by the nanocomplexes for ferroptosis induction in HCC cells.

With reduced GPX4 expression, accumulation of lipid peroxides occurs, which leads to cell membrane damage and ferroptosis occurrence. Further quantification of lipid peroxide accumulation was performed by BODIPY C11 staining coupled with flow cytometry analysis in Bel-7402 cells after 48 h of treatment with GOA/miR-363-5pi or GOA/miR-765i nanocomplexes. In comparison to those of the control and free miR groups, elevated levels of lipid peroxides were noticed in both Gem and GOA groups, which could potentially be attributed to an imbalance in the intracellular redox equilibrium caused by cytotoxicity of gemcitabine (Fig. 5F). Furthermore, the GOA/miR-363-5pi or GOA/miR-765i nanocomplexes exhibited FCM intensities 1.5-fold greater than that of the GOA group, indicating the miR delivery can effectively upregulate the lipid peroxide levels for further triggering ferroptosis in cancer cells in turn.

Finally, to confirm the occurrence of ferroptosis in Bel-7402 cells, a rescue experiment with ferrostatin-1 (Fer-1), a ferroptosis inhibitor, was performed after GOA/miR-363-5pi or GOA/miR-765i nanocomplex treatment. At 48 h and 72 h of incubation, the co-administration of Gem, GOA micelles, and GOA/miR-NC nanocomplex with Fer-1 did not enhance cell viability relative to Fer-1 alone, indicating gemcitabine alone could not trigger ferroptosis. Conversely, Fer-1 reversed the decreased viability of Bel-7402 cells treated with either GOA/miR-363-5pi or GOA/miR-765i nanocomplexes ($p<0.001$, Fig. 5G), suggesting that the cell death mode induced by miR-363-5pi or miR-765i was indeed ferroptosis. It is noteworthy that the transfection of miR-765i induced ferroptosis effects that were essentially identical to those of miR-363-5pi, which may be explained by the comparable upregulated LHPP protein expression levels by both miRNAs.

Collectively, the potent anti-HCC effects of GOA/miR-363-5pi and GOA/miR-765i nanocomplexes were primarily attributed to the combination of gemcitabine-induced chemotherapy and miR-mediated ferroptosis, which upregulates LHPP expression and inactivates the PI3K/Akt pathway. We, therefore, draw a conclusion that GOA/miR-363-5pi and GOA/miR-765i nanocomplexes

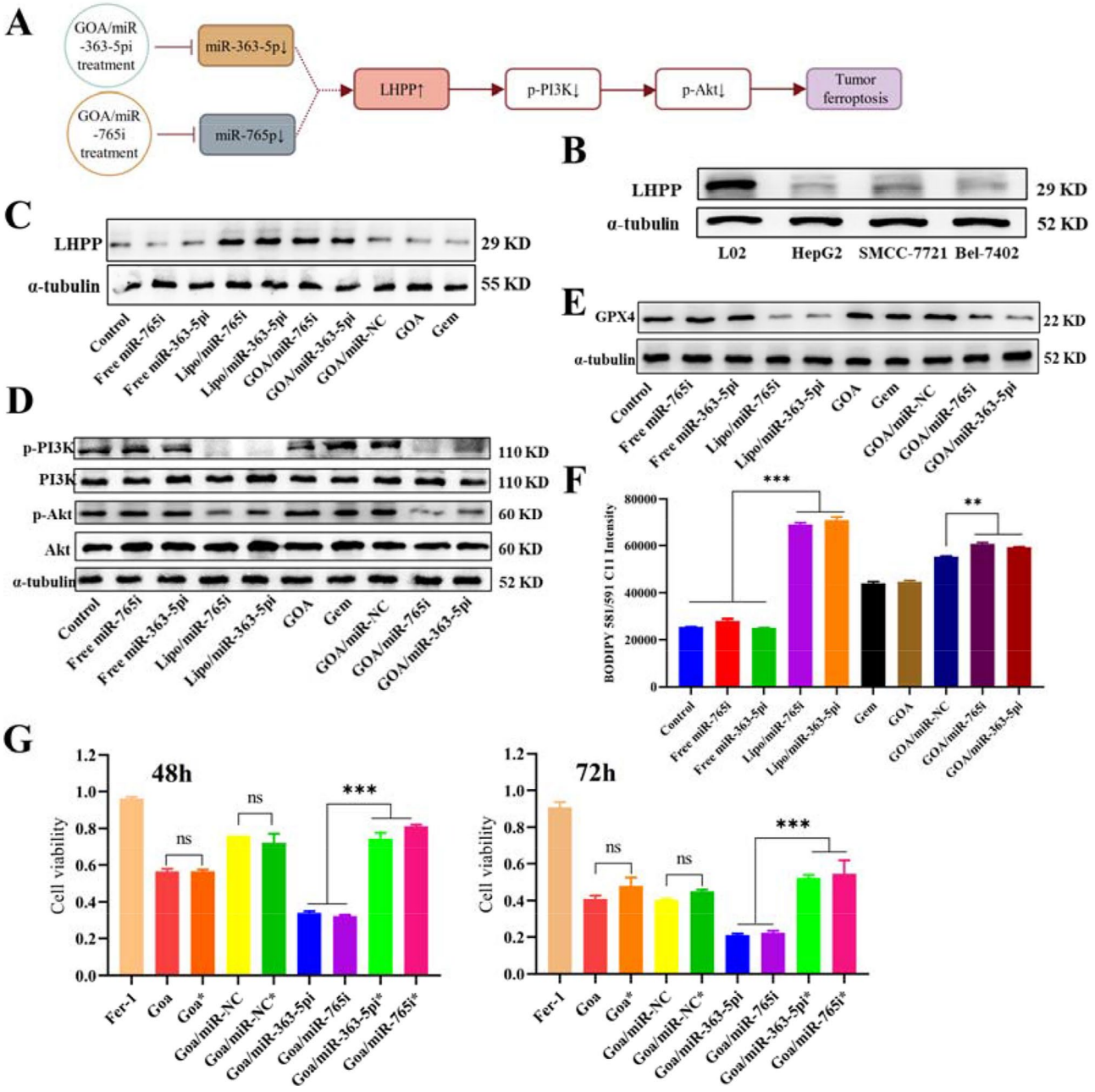

Fig. 5 In vitro antitumor mechanism. (**A**) Schematic illustration of the ferroptosis-induced mechanism after GOA/miR-363-5pi or GOA/miR-765i nanocomplex treatment. (**B**) LHPP expression in three HCC cell lines. (**C**) The expression of LHPP in Bel-7402 cells after treatment with different component formulations. (**D**) The protein levels of total PI3K (PI3K), phosphorylated PI3K (p-PI3K), total AKT (AKT), and phosphorylated AKT (p-AKT) were determined by Western blotting. (**E**) Expression of GPX4 in Bel-7402 cells after 48-hour treatment with different formulations. (**F**) Intracellular lipid accumulation was assessed by flow cytometry following staining with BODIPY in Bel-7402 cells after treatment with different formulations. (**G**) Ferroptosis inhibitors ferrostatin-1 (*) rescue Bel-7402 cell death induced by GOA/miR-363-5pi or GOA/miR-765i nanocomplex at 48 h and 72 h. Data represent mean ± s.d. ($n = 3$). $^{**}p < 0.01$, $^{***}p < 0.001$, ns: not significant

serve as ferroptosis inducers in the absence of ferrous nanoparticles.

In vivo anti-HCC effects

Effective tumor tissue accumulation is a prerequisite for anti-HCC effects. Cy5.5 was used as a fluorescent dye to label the nanocomplexes via physical encapsulation. The resulting Cy-5.5-labelled nanocomplexes, GOA/miR-Cy5.5 underwent tail vein injection in BALB/c nude mice bearing Bel-7402 tumor xenografts, and the fluorescence distributions in major organs and tumors were subsequently visualized in a FUSION FX imaging system

(VilberLourmat, France) (Fig. S6A). The fluorescence intensity of Cy5.5 reached a peak value at about 8 h post injection and completely disappeared after 24 h in the tumor site (Fig. S6B), indicating that the GOA/miR-Cy5.5 nanocomplex could effectively accumulate in the tumor through passive targeting via an EPR effect. Similar time-dependent fluorescence intensity changes were recorded in the major organs (Fig. S6C). The biodistribution data reveal that GOA/miR nanocomplex had the potential to target HCC without damaging normal organs.

Encouraged by GOA/miR nanocomplex biodistribution results, the antitumor effects of GOA/miR nanocomplex were further evaluated in the BALB/c nude mice bearing Bel-7402 tumor xenografts. Six groups of tumor-bearing mice were intravenously injected with saline, Gem, GOA micelles, GOA/miR-NC nanocomplex, GOA/miR-363-5pi nanocomplex, and GOA/miR-765i nanocomplex at 48-hour intervals for a total of five administrations (Fig. 6A). Compared to the saline group, both free gemcitabine and all GOA-based formulations exhibited significant inhibitory effects on tumor growth (Fig. 6B). In contrast to the GOA/miR-NC nanocomplex, both GOA/miR-363-5pi and GOA/miR-765i nanocomplexes exhibited almost flattened tumor growth profiles ($p<0.001$). Mice treated with GOA/miR-363-5pi and GOA/miR-765i nanocomplexes showed 88% and 89% regression in tumor volumes, respectively, which were significantly higher than those of Gem (46%), GOA micelles (66%), and GOA/miR-NC nanocomplex (66%) groups (Fig. 6C). The excellent treatment efficiency of both nanocomplexes was further supported by the photographs of ex vivo tumor tissues (Fig. 6D) and the average weight of the tumor tissues (Fig. 6E) extracted from the mice sacrificed on the 11th day. Consistent with the in vitro findings, miR-765i showed in vivo anti-tumor efficacy almost identical to that of miR-363-5p.

In vivo LHPP expression and ferroptosis induction

An in-depth investigation of the in vivo antitumor mechanism of GOA/miR-363-5pi and GOA/miR-765i nanocomplexes was finally conducted. In line with the in vitro results, the immunohistochemistry images of tumor tissues indicated significant upregulation of LHPP expression following treatment with either the GOA/miR-363-5pi or GOA/miR-765i nanocomplexes, compared to those of Gem, GOA micelles, and GOA/miR-NC nanocomplex (Fig. 7A). This observation was further supported by the higher average OD value of LHPP, as determined by the semi-quantitative immunohistochemical analysis ($p<0.001$, Fig. 7B). The elevated LHPP expression mainly resulted from the successful delivery of miR-363-5pi and miR-765i via the GOA/miR nanocomplex.

The specific ferroptosis markers, including the level of GPX4 and lipid peroxidation in tumor tissues, were assessed using immunohistochemistry and flow cytometry, respectively. In contrast to the observed LHPP expression trend, a decreased GPX4 expression was noticed in tumor tissues treated with the GOA/miR-363-5pi and GOA/miR-765i nanocomplexes compared to those of the other groups (Fig. 7A), which was further confirmed by a semi-quantitative analysis of fluorescence intensity (Fig. 7C). Furthermore, the lipid peroxidation levels in mice tumor tissue treated with GOA/miR-363-5pi and GOA/miR-765i nanocomplexes were approximately ~ 1.37 and 1.41-fold higher than that of the control group, respectively (Fig. 7D). These values were significantly greater than those observed of the mice tumor tissue treated with Gem (~ 1.01-fold), GOA micelles (~ 1.19-fold), and GOA/miR-NC nanocomplex (~ 1.21-fold) ($p<0.001$). Consistent with the in vitro findings, miR-765i had an upregulation effect on LHPP expression in vivo similar to that of miR-363-5p, suggesting the similar potencies of the two miRNAs in ferroptosis induction. Collectively, the aforementioned biological evidence supports GOA/miR-363-5pi or GOA/miR-765i nanocomplexes-mediated effective ferroptosis via LHPP protein expression upregulation.

The enhanced therapeutic efficacy of the GOA/miR-363-5pi and GOA/miR-765i nanocomplexes, compared to those of the other groups, is reasonably attributed to the successful co-delivery of miR-363-5pi or miR-765i with Gem. Therefore, the delivery system plays an important role in mediating combinatory therapy via simultaneous LHPP-triggered ferroptosis and GOA-induced chemotherapy, outperforming the efficacy of chemotherapy alone, for enhanced treatment of HCC.

In vivo safety assessment

The in vivo biosafety of nano-inducers, such as GOA/miR-363-5pi and GOA/miR-765i nanocomplexes, is of paramount concern. Body weights were measured every 2 days, as a decreased body weight profile was an obvious indication of severe toxicity. In the whole experimental period, insignificant changes in mice weights were observed after treatment with the GOA-based nanocomplexes whereas substantial weight losses were noticed after 4 days of Gem treatment, highlighting the superior biosafety of the nanocomplex (Fig. 8A).

Due to Gem's tendency to induce hemotoxic side effects in clinics, blood samples were collected and analyzed from mice treated with different formulations for 11 days. No observable damage to red or white blood cells was evident in any of the experimental groups (Fig. S7). However, the number of platelets was decreased in the Gem group, a well-known toxic side effect in clinical settings. Notably, this decline was prevented by

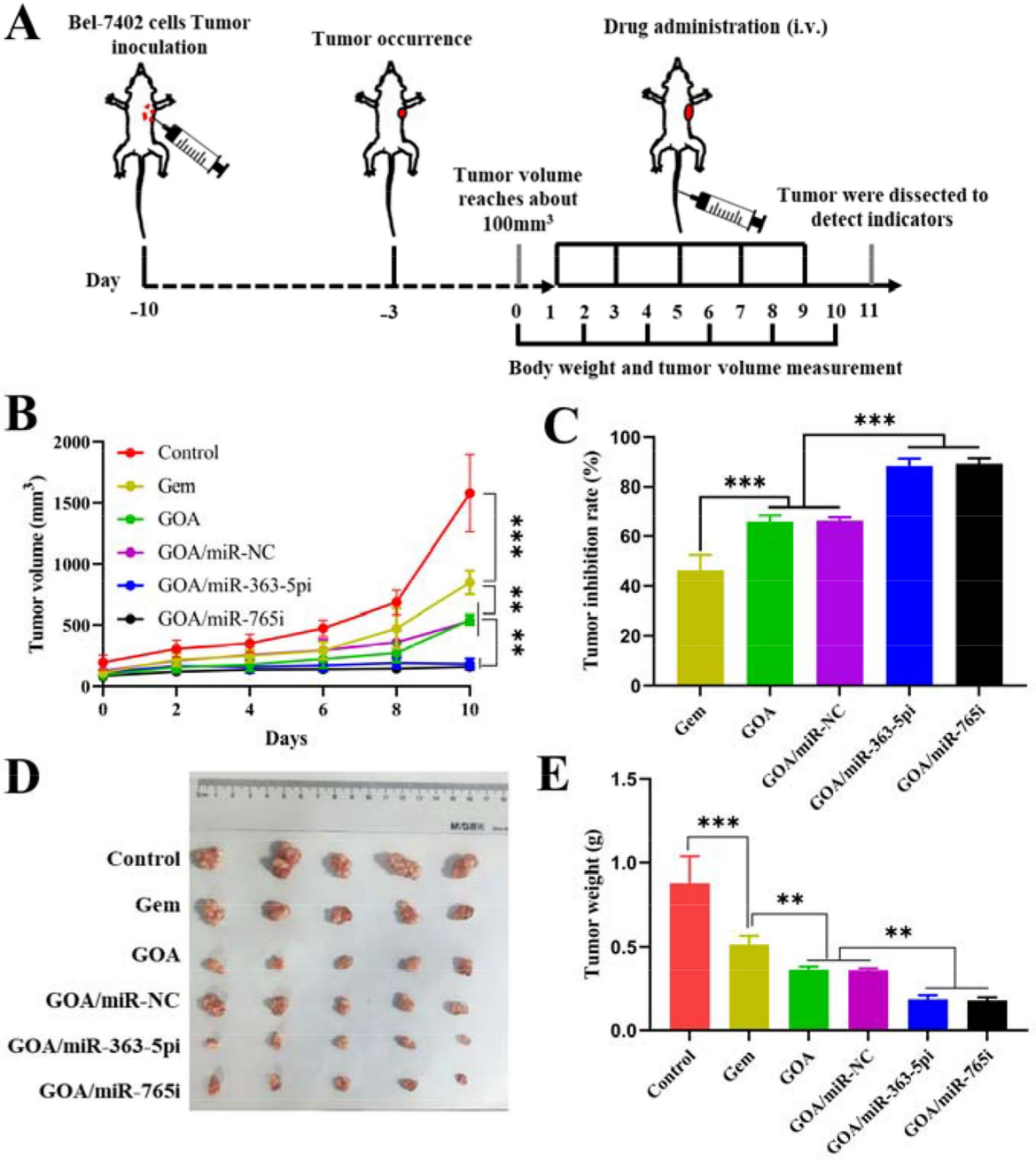

Fig. 6 In vivo evaluation of the therapeutic effects of GOA/miR-363-5pi and GOA/miR-765i nanocomplexes in HCC treatment. (**A**) Experiment schedule of anti-tumor study in Bel-7402-tumor-bearing BALB/c mice. (miRNA dose: 1 mg/kg, administered intravenously every 2 days for a total of 5 doses). (**B**) Tumor volume and (**C**) tumor inhibition rate of Bel-7402 tumor-bearing BALB/c mice treated with different formulations. (**D**) Photographs and (**E**) tumor weight of ex vivo tumor tissues at the end of treatment. Data represent mean ± s.d. ($n = 5$). $^{**}p < 0.01$, $^{***}p < 0.001$

GOA-based formulations, likely due to the precise drug delivery of the nanocomplex for minimized accumulation at the non-target site, and the noncationic properties of GOA-based formulations for reduced nanocomplex toxicity to cell membranes (Fig. 8B). Overall, the intravenous injection of GOA/miR-363-5pi and GOA/miR-765i nanocomplexes did not induce any detrimental effects on blood cell counts.

Finally, histological analysis of tumor tissues and vital organs, including the heart, liver, and kidney, was performed using H&E staining. The major organs exhibited no evident pathological abnormalities. As expected, the tumor tissues of nude mice treated with the GOA/miR nanocomplex displayed more obvious cytoplasmic disappearance, karyopyknotic, and apoptosis (indicated as arrows) compared to those of the other groups (Fig. 8C).

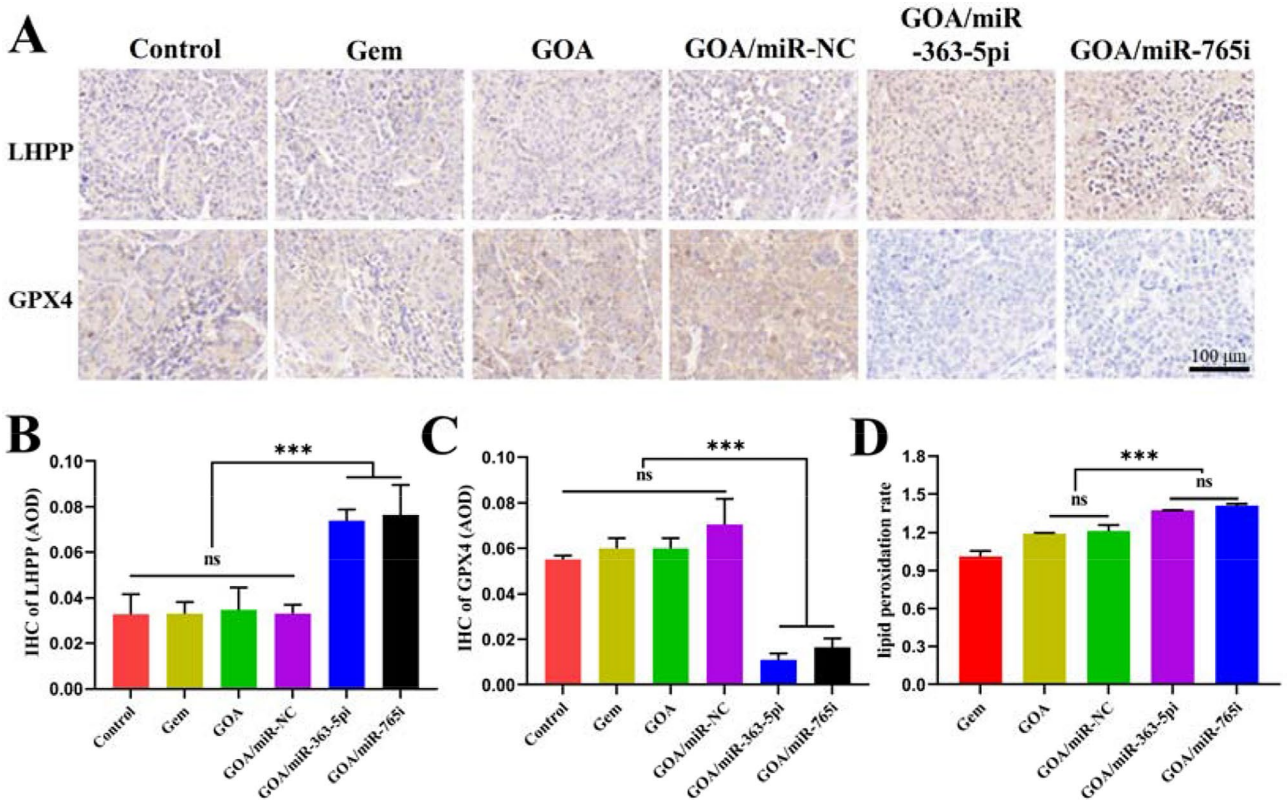

Fig. 7 In vivo ferroptosis induced by the treatment of GOA/miR-363-5pi and GOA/miR-765i nanocomplex. (**A**) Immunohistochemistry assay of LHPP and GPX4 expression in tumor tissues from Bel-7402-tumor-bearing BALB/c mice. (**B**) Semiquantitative analysis of immunohistochemical AOD for LHPP and (**C**) GPX4 by using Image J software. (**D**) Relative quantification of peroxidized lipids accumulated in the tumor tissues was analyzed through flow cytometry. Data represent mean ± s.d. ($n = 5$). ***$p < 0.001$

No significant difference in serum inflammatory factors IL-6 and IFN-α was observed between the all of groups, confirming that GOA/miR-363-5pi and GOA/miR-765i nanocomplexes did not lead to a systemic inflammatory response (Fig. S8). Therefore, the application of GOA/miR-363-5pi and GOA/miR-765i nanocomplexes demonstrated significant antitumor efficacy while minimizing systematic toxicity on normal organs and tissues for enhanced potential suitability for in vivo applications.

Potential for immune activation

Currently, the induction of immunogenic cell death (ICD) by combining multiple therapies is an incredibly promising approach for advancing cancer therapy. To assess the immune activation potential of the GOA/miR-363-5pi nanocomplex, the release of damage-associated molecular patterns (DAMPs), which serve as a signature for immunogenic cell death (ICD), was investigated in Bel-7402 cells treated with nanocomplex. The strongest calreticulin (CRT) fluorescence, as well as the lowest HMGB1 fluorescence, could be clearly observed after GOA/miR-363-5pi and GOA/miR-765i nanocomplexes treatments (Fig. 9A), which demonstrated that the synergistic strategy of chemotherapy and ferroptosis triggered by GOA/miR-363-5pi nanocomplex stimulated effective CRT exposure and HMGB1 release. In addition, extracellular HMGB1 (Fig. 9B) and ATP (Fig. 9C) concentrations were significantly enhanced in the GOA/miR-363-5pi and GOA/miR-765i nanocomplexes groups than those in the Gem, GOA, and GOA/miR-NC nanocomplex groups ($p < 0.001$) detected by Elisa kit, which demonstrated that GOA/miR-363-5pi nanocomplex stimulated HMGB1 and ATP release from Bel-7402 cells into the extracellularly. Thus, the GOA/miR-363-5pi nanocomplex possesses the capacity to induce ICD through the stimulation of DAMPs release, which holds the potential to activate anti-tumor immune response.

Conclusion

In summary, two nano-inducers, the GOA/miR-363-5pi and GOA/miR-765i nanocomplexes, were successfully fabricated through hydrogen bonding and hydrophobic interactions for the synergistic treatment of HCC via chemotherapy and ferroptosis. These nano-inducers effectively encapsulated miRNA inhibitors, achieving a negative surface potential of -21.5 mV, attributed to the formation of specific hydrogen bonds, which contributed to their exceptional stability and biosafety profiles. Most

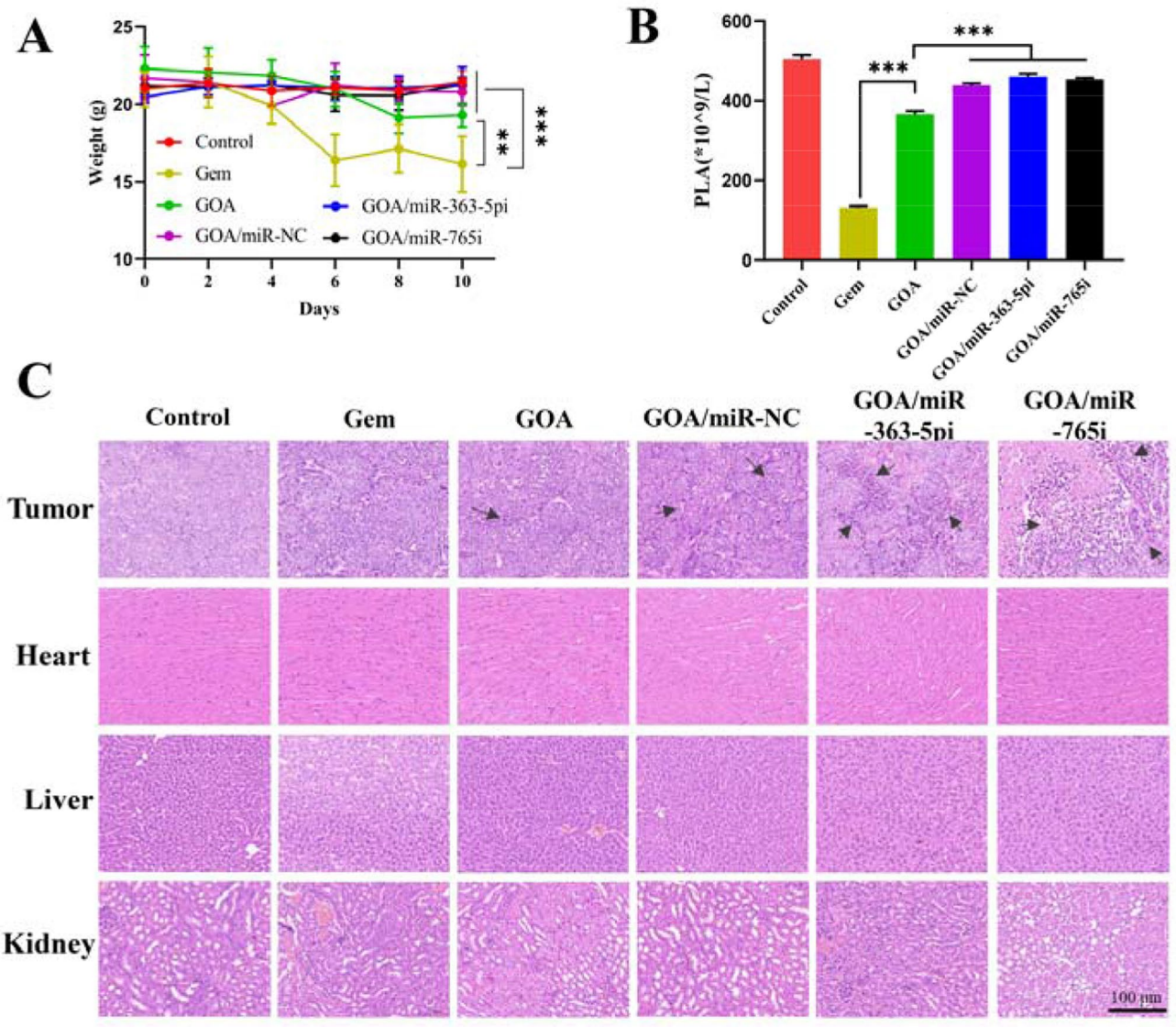

Fig. 8 In vivo safety assessment of different formulations in BALB/c nude mice bearing Bel-7402 xenograft model. (**A**) Body weight of Bel-7402-tumor-bearing BALB/c nude mice treated with different formulations. (**B**) The levels of platelet in the serum after treatment on the 11th day. (**C**) H&E staining of the tumor, heart, liver, and kidney (scale bars: 100 μm). Data represent mean ± s.d. ($n = 5$). $^{**}p < 0.01$, $^{***}p < 0.001$

importantly, the GOA/miR-363-5pi nanocomplex demonstrated superior tumor suppressive effects and held great potential as a HCC treatment strategy by combining LHPP-induced ferroptosis with GOA-mediated chemotherapy without any iron toxicity. Ferroptosis plays a crucial role in tumorigenesis and progression, and several drugs targeting ferroptosis have entered clinical trials [29]. For example, Xu et al. confirmed miR-1287-5p-induced ferroptosis [30]. Triggering ferroptosis via miRNAs has been a potential strategy to enhance single chemotherapy regimens [31]. Therefore, this study not only offers a novel strategy to transform synergistic chemotherapy with gene therapy into tumor immunogenicity ferroptosis but also elucidates the underlying crosstalk between LHPP and ferroptosis, paving the way for a novel therapeutic approach in the clinical management of HCC.

However, a non-ferrous ferroptosis approach also has some inherent limitations. Firstly, although the ICD-inducing potential of GOA/miR-353-5pi has been reported, we could not further evaluate in vivo whether GOA/miR-353-5pi could activate a complete ICD response because Bel-7402 cells are derived from a human hepatocellular carcinoma cell line. Secondly, the relatively small sample size and the lack of long-term toxicity assessment limit our anticipation whether the same results would be observed in human operating systems. Further collection of HCC patient samples seems a reliable approach to verify the accuracy of this critical point. Last but not least, the use of GOA/miR-353-5pi

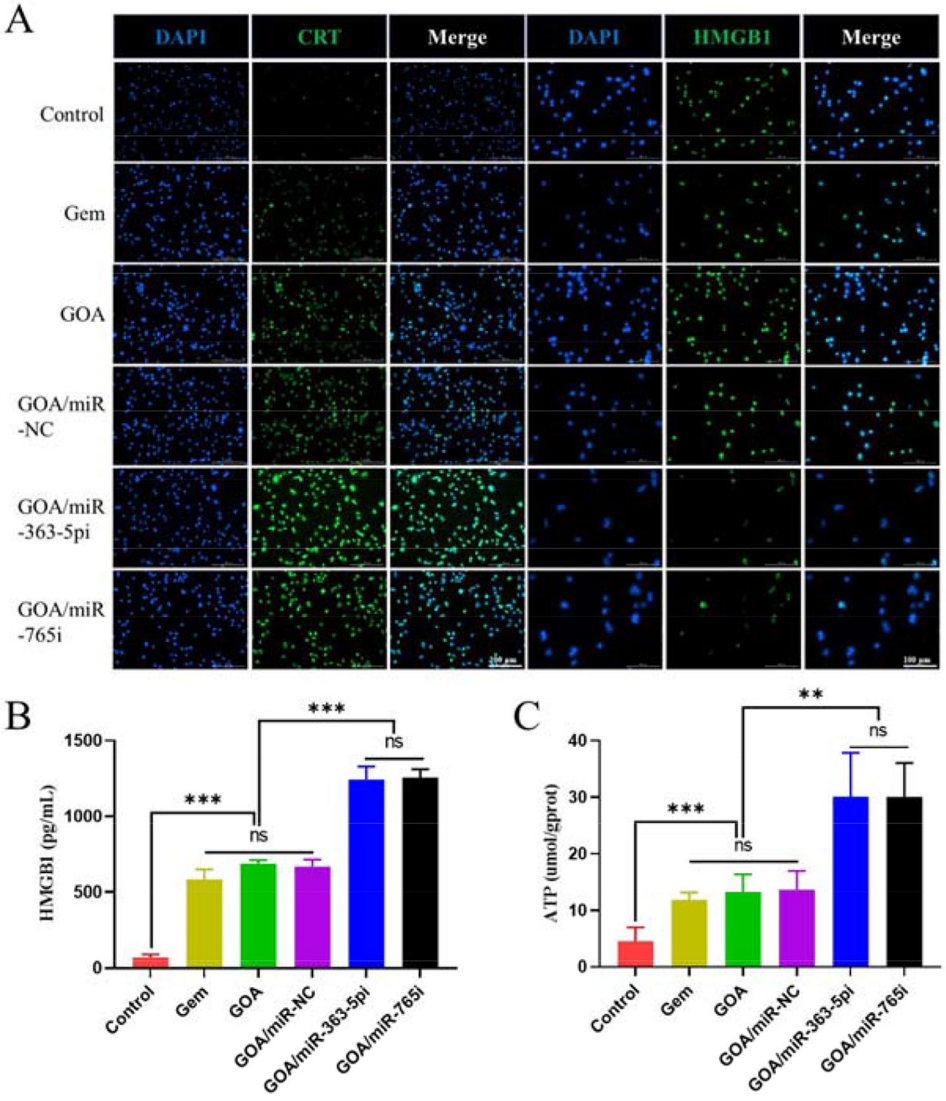

Fig. 9 Assessment of immunogenic cell death of GOA/miR nanocomplex. (**A**) The represent image of CRT (scale bars: 200 μm) and HMGB1 (scale bars: 100 μm) detected by fluorescence microscope in Bel-7402 cells after treatment by GOA/miR-363-5pi nanocomplex and GOA/miR-765i nanocomplex. Concentrations of (**B**) HMGB1 and (**C**) ATP in cell culture medium after treatment with each component. Data represent mean ± s.d. ($n = 3$). $^{**}p < 0.01$, $^{***}p < 0.001$, ns: not significant

nanocomplex possible biosafety profiles requires extensive in-depth clinical studies. In summary, more relevant studies are needed to further reveal and elaborate the relationship between LHPP, ferroptosis and miRNAs, which could potentially improve the treatment of HCC patients.

Materials and methods

Materials

Gemcitabine (Gem) was purchased from J&K Scientific LTD (Beijing, China). MiRNA −363-5p inhibitor mimics (sequence: 5' – AAA UUG CAU CGU GAU CCA CCC G −3', miR −363-5pi), miRNA-765 inhibitor mimics (sequence:5' – CAU CAC CUU CCU UCU CCU CCA −3', miR-765i) and negative control miRNA (sequence:5' – UUG UAC CAU ACA AAA GUA CUG −3', miR - NC), fluorescein-labeled miRNA were synthesized and purified by HPLC by GenePharm (Suzhou, China). Agarose was obtained from GENE COMPANY (Hong Kong, China); Hoechst 33,342 was purchased from Molecular Probes Inc. (Oregon, USA); (3 -(4, 5 -dimethyl thiazolyl −2) -2, 5 -diphenyltetrazolium bromide) (MTT) was purchased from Sigma Aldrich. Co. (St. Louis, MO). Lipofectamine 2000 (Lipo) was purchased from Invitrogen (USA). Antibodies was purchased from Abcam (UK).

HepG2, BEL-7402, and SMMC-7721 cells, were supplied by Shanghai Life Sciences Academe, Shanghai. Both fetal bovine serum (FBS) and Dulbecco's modified Eagle's medium (DMEM) were ordered from Gibco, America.

Preparation of GOA/miR nanocomplex

Gemcitabine-oleic acid materials (GOA) were prepared according to the previously reported procedures [6]. The synthetic details are described in Fig. S1. Briefly, the GOA/miRNA nanocomplex was prepared using a nanoprecipitation approach, together with high-temperature denaturation and low-temperature annealing processes. In this approach, the GOA prodrug (solvent DMSO) and miRNA (solvent H_2O) were mixed well in a solvent.

Subsequently, the temperature of the mixture was first increased to 94 ℃ and maintained for 5 min followed by cooling to 60℃ and keeping for 10 min to promote the formation of hydrogen bonds between the nucleobase heads of the GOA prodrug and miRNAs. Finally, the temperature was lowered to 37℃, and DMSO was gradually added to the aqueous solution (DMSO volume was less than 1‰).

GOA loaded with miR-NC was denoted as GOA/miR-NC nanocomplex and used as a negative control. Blank GOA nanoparticles self-assembled from GOA were denoted as GOA micelles.

To verify the successful GOA/miR preparation, various GOA/miR mixtures with different molar feed ratios in a range from 100:1 to 250:1 were mixed with the loading buffer, which was subjected to electrophoresis in 1% agarose gel containing 0.1% Gel Red at 120 V for 20 min. After electrophoresis, the image was obtained at 302 nm using a gel imaging system.

Characterization

The mean sizes and Zeta-potentials of the prepared GOA/miR-NC, GOA/miR-363-5pi, and GOA/miR-765i nanocomplex were determined by Dynamic light scattering (DLS, Zetasizer nanoparticle analyzer, Nano ZS-90, Malvern Instruments, UK).

For transmission electron microscope (TEM, Hitachi-4800, Hitachi Limited, Japan), freshly prepared GOA/miR-NC nanocomplex were carefully dropped onto a carbon-coated copper grid or a silicon pellet (25 mm^2) and then dried at room temperature overnight before measurements.

Stability and safety evaluations in vitro

The long-term stability properties of GOA/miR-NC nanocomplex solution were assessed by monitoring the time-dependent size changes using DLS. Briefly, GOA/miR-NC nanocomplex solution at a concentration of 2 μM was suspended in PBS (pH 7.4), and the mean sizes were measured every 24 h over 1 week.

A solution of parent GOA/miR with a maximum concentration of 2 μM was diluted using distilled water to create a range of concentration gradients. These gradients were then analyzed using DLS measurements to assess the stability of the particles upon dilution. Similarly, a solution of parent GOA/miR was diluted with different commonly used media to examine the colloidal stability in terms of serum and salt. Finally, a total volume of 20 μL of GOA/miR solution was suspended in 380 μL of saline, and the sizes of the suspensions were measured every 48 h for 2 weeks.

To evaluate the serum stability, 100 μL of GOA/miR-NC nanocomplex, Lipo/miR-NC, and free miR were mixed with an equivalent volume of FBS and further incubated at 37 ℃ respectively, using FBS as a blank control. At predetermined time intervals (0, 0.5, 2, 4, 24, and 48 h), the optical density (OD) values at 560 nm were detected on a microplate reader (Multiskan™ FC, Thermo Fisher Scientific – CN, China).

Flow cytometry

Human HCC cells were cultured in 6-well plates at a density of 2.5×105 cells per well and incubated at 37℃, 5% CO_2 for 24 h. After discarding the culture medium, 1 mL of fresh Opti-MEM was added to the cells. The Opti-MEM contained nanocomplex with FAM-labeled miRNA at different mole ratios but a fixed final concentration of 100 nM. The mixture was then incubated for an additional 4–8 h at 37 °C. Following the incubation, the cells were rinsed with cold PBS, and treated with trypsin, and the uptake of FAM-labeled miRNA was detected using flow cytometry (Agilent BioTek, China). The FITC channel was used to determine the in vitro uptake.

Fluorescence microscopy

Human HCC cells were inoculated into 6-well plates of 2.5×10^5 cells per well and incubated for 24 h. Similarly, the cells in the aforementioned groups were processed using flow cytometry. Following the washing of cells with PBS, a 4% paraformaldehyde solution was introduced for cellular fixation, left undisturbed for 10 min, and then discarded. Subsequently, the nuclei were stained with a DAPI staining solution, and the stained cells were examined using fluorescence microscopy (Biotek, USA).

Cytotoxicity assay

The MTT assay was implemented to assess the cytotoxicity of GOA/miR-363-5pi nanocomplex, GOA/miR-765i nanocomplex, GOA/miR-NC nanocomplex, GOA micelles, and Gem. Human Bel-7402 HCC cells were seeded in a 96-well plate at a density of 8×103 cells per well. PBS non-cultured cells were added to the outermost circle, while DMEM non-cultured cells served as the blank control group. The plate was then incubated at 37 °C for 24 h. Subsequently, DMEM was removed and replaced with 100 nM of miR-NC (solvent Opti-MEM) in each preparation. Opti-MEM was utilized as a control, whereas the negative control group and the blank control group were added with an equal volume of Opti MEM

medium and incubated for 8 h. After 8 h, the incubation was replaced with DMEM and continued for 24, 48, and 72 h. Finally, MTT solution (5 mg/mL) was added to each well, and the plate was incubated for 4 h. All the liquid was aspirated, and the appropriate volume of DMSO was added and shaken for 10 min.

The cell viability (%) was calculated according to the following formula: Cell viability (%) = [OD 490 (sample) / OD 490 (control)] × 100%, where OD 490 (sample) is the absorbance from the cells treated with various nanoparticles and OD 490 (control) is that from the cells treated with Opti -MEM.

Lipid peroxidation

Referring to flow cytometry for cell culture and drug administration, the drug-containing medium was aspirated after 8 h of incubation. Subsequently, BODIPY 581/591 C11 (solvent DMEM) was introduced and allowed to incubate for 0.5 h. Following this, the samples were washed, digested, centrifuged, and resuspended in PBS. Protected from light, the lipid peroxide level of each cell was then detected using the FITC channel of flow cytometry.

Animals

Four-week-old BALB/c female mice (20±2 g) were obtained from Hunan Slaughter Jingda Laboratory Animal Co. The in vivo anti-tumor effects of GOA/miR were measured using BEL-7402 tumor-bearing BALB/c nude mice that were injected subcutaneously with 5×10^6 cells in the armpit of their right front limb. Once the tumor volume reached approximately about 100 mm^3, the mice were randomly divided into six groups, each consisting of five mice: (1) Saline, (2) Gem, (3) GOA micelles, (4) GOA/miR-NC nanocomplex, (5) GOA/miR-363-5pi nanocomplex, (6) GOA/miR-765i nanocomplex. 0.2 mL of the above formulations (equivalent dose of miRNA :1 mg/kg) were given via tail vein injection every other day, respectively, and monitored for 11 days. The tumor volume and body weight of nude mice were regularly measured every other day using vernier calipers and electronic scales.

The following formula is used to calculate the tumor volume: tumor volume V (mm^3)=L (long diameter, mm) × S^2 (short diameter, mm^2)/ 2.

All experimental designs and protocols involving animals were approved by the Experimental Animal Ethics Committee of the University of South China, Hunan, People's Republic of China (approval 4304079008946) and complied with the National Institutes of Health and University of South China guidelines on the care and use of animals for scientific purposes.

The tumor-inhibition rate (TIR) of five groups (Gem, GOA micelles, GOA/miR-NC nanocomplex, GOA/miR-363-5pi nanocomplex, and GOA/miR-765i nanocomplex) was determined by the Eq.:

$$\mathrm{TIR} = (1 - \mathrm{V}/\mathrm{V}_0) \times 100\%$$

where V and V_0 represent the tumor volume of the experimental groups (Gem, GOA micelles, GOA/miR-NC nanocomplex, GOA/miR-363-5pi nanocomplex or GOA/miR-765i nanocomplex) and the corresponding control groups (saline) after entire treatment, respectively.

Statistical analysis

Data were presented as means±standard deviations (SD). Unpaired Student's t-test (two-tailed) was used for comparing two -groups and one-way ANOVA followed by Tukey's test was used for analyzing multiple -groups. Differences with $p<0.05$ were considered statistically significant. All statistical analyses were carried out using GraphPad Prism Software (Version 5.0, GraphPad Software, San Diego, CA).

Supplementary Information

The online version contains supplementary material available at https://doi.org/10.1186/s12951-024-02918-2.

Supplementary Material 1

Author contributions

Yang Qin and Yunxian Li completed the Synthesis of GOA. Jieqiong Wang, Jiaqi Wang, Zhuoyi Rong, Yunxian Li, Yao Cheng, and Zhenghao Tao contributed to the animal experiment. Yang Qin, Haitao Zhang, and Xiaoli Lin performed the studies and analyzed the data. Yang Qin wrote the initial draft. Haitao Zhang supported the valuable suggestion for revision. Haitao Zhang, Hua Wei, and Cui-Yun Yu revised the final draft.

Funding

This work was financially supported by the Hunan Science and Technology Innovation Leading Talent Project (2022RC3080), the National Natural Science Foundation of China (82373826), the Key R&D Program of Hunan Province (2021SK2036, 2023SK2043), Research Foundation of Education Bureau of Hunan Province (No. 21A0284), Natural Science Foundation of Hunan Province (2021JJ30603, 2022JJ40381, 2023JJ50138), Scientific Research Project of Hunan Provincial Health Commission (No. 202113021875), and the National Innovation and Entrepreneurship Training Program for College Students (No. 202210555093).

Data availability

Data is provided within the manuscript or supplementary information files.

Declarations

Ethics approval and consent to participate

All experimental designs and protocols involving animals were approved by the Experimental Animal Ethics Committee of the University of South China, Hunan, People's Republic of China (approval 4304079008946) and complied with the National Institutes of Health and University of South China guidelines on the care and use of animals for scientific purposes.

Consent for publication

All authors have approved the manuscript be submitted.

Competing interests
The authors declare no competing interests.

Author details
[1]Pharmaceutical and Biomedical Polymers Research Laboratory, Institute of Pharmacy & Pharmacology, Hunan Province Cooperative Innovation Center for Molecular Target New Drug Study, School of Pharmaceutical Science & MOE Key Lab of Rare Pediatric Disease, Hengyang Medical School, University of South China, Hengyang 421001, China
[2]Affiliated Hospital of Hunan Academy of Chinese Medicine, Hunan Academy of Chinese Medicine, Changsha 410006, China

Received: 29 May 2024 / Accepted: 9 October 2024
Published online: 15 October 2024

References

1. Forner A, Reig M, Bruix J. Hepatocellular carcinoma. Lancet. 2018;391:1301–14.
2. Qin Y, Zhang H, Li Y, Xie T, Yan S, Wang J et al. Promotion of ICD via Nanotechnology. Macromol Biosci. 2023;23:e2300093.
3. Bray F, Laversanne M, Sung H, Ferlay J, Siegel RL, Soerjomataram I et al. Global cancer statistics 2022: GLOBOCAN estimates of incidence and mortality worldwide for 36 cancers in 185 countries. CA Cancer J Clin. 2024;74:229–263.
4. Huang C, Xie T, Liu Y, Yan S, OuYang F, Zhang H et al. A Sodium Alginate-based multifunctional nanoplatform for synergistic chemo-immunotherapy of Hepatocellular Carcinoma. Adv Mater. 2023;35:e2301352.
5. Wang YQ, Huang C, Ye PJ, Long JR, Xu CH, Liu Y, Ling XL, Lv SY, He DX, Wei H, Yu CY. Prolonged blood circulation outperforms active targeting for nanocarriers-mediated enhanced hepatocellular carcinoma therapy in vivo. J Control Release. 2022;347:400–13.
6. Zhang HT, Sun J, Yan Y, Cui SH, Wang H, Wang CH, Qiu C, Chen X, Ding JS, Qian HG, et al. Encapsulated microRNA by gemcitabine prodrug for cancer treatment. J Control Release. 2019;316:317–30.
7. Jiang X, Stockwell BR, Conrad M. Ferroptosis: mechanisms, biology and role in disease. Nat Rev Mol Cell Biol. 2021;22:266–82.
8. Chen X, Kang R, Kroemer G, Tang D. Broadening horizons: the role of ferroptosis in cancer. Nat Rev Clin Oncol. 2021;18:280–96.
9. Tang D, Chen X, Kang R, Kroemer G. Ferroptosis: molecular mechanisms and health implications. Cell Res. 2021;31:107–25.
10. Zhang C, Bu W, Ni D, Zhang S, Li Q, Yao Z, Zhang J, Yao H, Wang Z, Shi J. Synthesis of Iron Nanometallic glasses and their application in Cancer Therapy by a localized Fenton Reaction. Angew Chem Int Ed Engl. 2016;55:2101–6.
11. Lin L, Wang S, Deng H, Yang W, Rao L, Tian R, Liu Y, Yu G, Zhou Z, Song J, et al. Endogenous Labile Iron Pool-mediated free Radical Generation for Cancer Chemodynamic Therapy. J Am Chem Soc. 2020;142:15320–30.
12. Zhu L, You Y, Zhu M, Song Y, Zhang J, Hu J, Xu X, Xu X, Du Y, Ji J. Ferritin-hijacking nanoparticles spatiotemporally directing endogenous ferroptosis for synergistic anticancer therapy. Adv Mater. 2022;34:e2207174.
13. Hindupur SK, Colombi M, Fuhs SR, Matter MS, Guri Y, Adam K, Cornu M, Piscuoglio S, Ng CKY, Betz C, et al. The protein histidine phosphatase LHPP is a tumour suppressor. Nature. 2018;555:678–82.
14. Wang X, Cheng H, Zhao J, Li J, Chen Y, Cui K, Tian L, Zhang J, Li C, Sun S, et al. Long noncoding RNA DLGAP1-AS2 promotes tumorigenesis and metastasis by regulating the Trim21/ELOA/LHPP axis in colorectal cancer. Mol Cancer. 2022;21:210.
15. Hou B, Li W, Xia P, Zhao F, Liu Z, Zeng Q, Wang S, Chang D. LHPP suppresses colorectal cancer cell migration and invasion in vitro and in vivo by inhibiting Smad3 phosphorylation in the TGF-β pathway. Cell Death Discov. 2021;7:273.
16. Yi J, Zhu J, Wu J, Thompson CB, Jiang X. Oncogenic activation of PI3K-AKT-mTOR signaling suppresses ferroptosis via SREBP-mediated lipogenesis. Proc Natl Acad Sci U S A. 2020;117:31189–97.
17. Meng Y, Cao J, Li Y, Duan S, Zhou Z, Li J, Ousmane D, Ou C, Wang J. Emerging role of ferroptosis-related circular RNA in tumor metastasis. Front Pharmacol. 2023;14:1168458.
18. Tian Z, Yu T, Wei H, Ning N. Clinical value of LHPP-associated microRNAs combined with protein induced by vitamin K deficiency or antagonist-II in the diagnosis of alpha-fetoprotein-negative hepatocellular carcinoma. J Clin Lab Anal. 2020;34:e23071.
19. Diener C, Keller A, Meese E. Emerging concepts of miRNA therapeutics: from cells to clinic. Trends Genet. 2022;38:613–26.
20. Rupaimoole R, Slack FJ. MicroRNA therapeutics: towards a new era for the management of cancer and other diseases. Nat Rev Drug Discov. 2017;16:203–22.
21. Zhu J, Yang S, Qi Y, Gong Z, Zhang H, Liang K, Shen P, Huang YY, Zhang Z, Ye W, et al. Stem cell-homing hydrogel-based miR-29b-5p delivery promotes cartilage regeneration by suppressing senescence in an osteoarthritis rat model. Sci Adv. 2022;8:eabk0011.
22. Phung CD, Nguyen HT, Choi JY, Pham TT, Acharya S, Timilshina M, Chang JH, Kim JH, Jeong JH, Ku SK, et al. Reprogramming the T cell response to cancer by simultaneous, nanoparticle-mediated PD-L1 inhibition and immunogenic cell death. J Control Release. 2019;315:126–38.
23. Ning Q, Liu YF, Ye PJ, Gao P, Li ZP, Tang SY, He DX, Tang SS, Wei H, Yu CY. Delivery of liver-specific miRNA-122 using a targeted Macromolecular Prodrug toward Synergistic Therapy for Hepatocellular Carcinoma. ACS Appl Mater Interfaces. 2019;11:10578–88.
24. Zhang S, Gao H, Bao G. Physical principles of Nanoparticle Cellular endocytosis. ACS Nano. 2015;9:8655–71.
25. Sahay G, Alakhova DY, Kabanov AV. Endocytosis of nanomedicines. J Control Release. 2010;145:182–95.
26. Gilleron J, Querbes W, Zeigerer A, Borodovsky A, Marsico G, Schubert U, Manygoats K, Seifert S, Andree C, Stöter M, et al. Image-based analysis of lipid nanoparticle-mediated siRNA delivery, intracellular trafficking and endosomal escape. Nat Biotechnol. 2013;31:638–46.
27. Rennick JJ, Johnston APR, Parton RG. Key principles and methods for studying the endocytosis of biological and nanoparticle therapeutics. Nat Nanotechnol. 2021;16:266–76.
28. Chen D, Chu B, Yang X, Liu Z, Jin Y, Kon N, Rabadan R, Jiang X, Stockwell BR, Gu W. iPLA2β-mediated lipid detoxification controls p53-driven ferroptosis independent of GPX4. Nat Commun. 2021;12:3644.
29. Shi TM, Chen XF, Ti H. Ferroptosis-based therapeutic strategies toward Precision Medicine for Cancer. J Med Chem. 2024;67:2238–63.
30. Xu Z, Chen L, Wang C, Zhang L, Xu W. MicroRNA-1287-5p promotes ferroptosis of osteosarcoma cells through inhibiting GPX4. Free Radic Res. 2021;55:1119–29.
31. Jiang M, Jike Y, Liu K, Gan F, Zhang K, Xie M, Zhang J, Chen C, Zou X, Jiang X, et al. Exosome-mediated mir-144-3p promotes ferroptosis to inhibit osteosarcoma proliferation, migration, and invasion through regulating ZEB1. Mol Cancer. 2023;22:113.

Publisher's note